JOURNAL OF MATERIALS SCIENCE 32 (1997) 1915–1924

Combustion synthesis and structure formation in a model Cr–CrO_3 self-propagating high-temperature synthesis system

V. I. YUKHVID, S. V. MAKLAKOV, P. V. ZHIRKOV, V. A. GORSHKOV, N. I. TIMOKHIN, A. Y. DOVZHENKO
Institute for Structural Macrokinetics (ISMAN), Russian Academy of Sciences, 142 432 Chernogolovka, Moscow Region, Russia

The combustion synthesis (self-propagating high-temperature synthesis, SHS) of a model Cr–CrO_3 system is studied both experimentally and theoretically. The system is chemically simple, i.e. it is composed of only two elements, and convenient for combustion and phase formation studies. A new combustion model for a ''metal–metal oxide'' system and a mathematical model of phase and structure formation are developed. A number of dependencies are determined in the experiments and are described in the combustion model. It is shown that the leading combustion stage is the gas phase oxidation reaction. Different types of microstructures formed from homogeneous melt are revealed. A qualitative agreement between experimental data, theoretical analysis and calculation results is obtained.

1. Introduction

Self-propagating high-temperature synthesis (SHS) also known as combustion or self-sustained synthesis comprises a large field of experimental and theoretical investigations based on combustion theory, materials science, macrokinetics, inorganic chemistry and other related sciences. The literature on the subject is quite extensive, thus we restrict our attention to the reviews available. The discovery of SHS and the earliest studies of this new phenomenon were made in the USSR by Merzhanov and his coworkers in the early 1970s [1]. Then, American and Japanese researchers became involved in the problem [2–4]. Impressive results have been achieved in the technological application of this method for production of various inorganic compounds, powders, coatings, monoliths, etc. [5, 6].

In this paper we have studied the combustion synthesis of a model Cr–CrO_3 SHS system. Combustion of systems, i.e. metal oxide–metal reductant, is widely used not only in SHS [5] but in metallurgy [7, 8] and pyrotechnics [9–11]. This system is a convenient model for studying combustion and, especially, structure formation. It is a most simple model from the chemical point of view: only two elements are involved, chromium and oxygen. This fact is an essential simplification in order to understand the intrinsic mechanism of such a multistage and complicated process as combustion synthesis.

2. Experimental procedure

Polydispersional chromium anhydride (CrO_3; analytical grade; with diameter, $d_{CrO_3} < 300$ μm) and polydispersional chromium powders (PKhS1 and KhR-0000, $d_{Cr} < 120$ μm, with a narrow size distribution) were used in the experiments.

The ratio CrO_3 : Cr was changed in a wide range: $0.14 < \alpha < 0.85$ (α is the mass portion of chromium, $\alpha = 0.34$ being the stoichiometric composition). In this case, the stoichiometric composition is that in which the amount of oxygen is sufficient for achieving complete oxidation of chromium

$$CrO_3 + Cr \rightarrow Cr_2O_3 \quad (1)$$

Mixtures with $\alpha < 0.34$ and $\alpha > 0.34$ contain a surplus and a deficiency of oxygen, respectively.

Before combustion, the mixture was set into a refractory crucible and pressed manually. Under such an arrangement, the density is slightly dependent on the dispersity of the components and is 2.3–2.4 g cm^{-3} when α varies from 0.14 up to 0.83.

Due to high hydroscopicity, the sample was dried at 100 °C for 8 h. All operations of weighing, mixing and arranging of the crucibles were fulfilled in an hermetically sealed room in a dry atmosphere. The compositions were mixed in a tumble roller for 2 h.

Cylindrical quartz vessels with 20 mm inner diameters, 1.5–2 mm wall thickness and 40 mm height were used to make camera recordings of the combustion. In the experiments the initial mass of the mixture was 25–35 g. The experiments were realized in a vessel of constant pressure in argon atmosphere under a pressure, P_0, ranging from 0.1 to 13.2 MPa. During combustion the pressure inside the vessel was kept constant by means of a release valve.

0022–2461

Linear combustion velocity, U_0, depth of mixture spraying under combustion η_p, sample shrinkage, h_s, as well as the chemical composition of the combustion products were determined in experiments. U_0 was measured using a low motion camera FR-11 by the standard technique. η_p and h_s were calculated using formulae

$$\eta_p = (M_0 - M_k)/M_0 \qquad h_s = h/h_0$$

where M_0 and M_k are the masses and h_0 and h are the heights of the initial mixture and the combustion products in the vessel, correspondingly.

Cr and O contents in the samples were measured using conventional methods of chemical and X-ray analysis. Visual observation and analysis of the camera recording diagrams demonstrate

1. the system "CrO_3–Cr" is able to burn within the pressure range ($P_0 = 0.1$–13.2 MPa) and chromium size range ($d_{Cr} = 30$ μm) studied;
2. the ratio of components limits combustion ($\alpha = 0.14$ and $\alpha = 0.83$);
3. the combustion proceeds in a mode close to steady state with a plane front;
4. when $0.72 < \alpha < 0.83$, combustion is followed by a weak glowing, i.e. smouldering combustion;
5. when $0.14 < \alpha < 0.16$, combustion proceeds in a spinning mode.

The experimental results are shown in Figs 1–7. Every point in the plots was defined for two to three experiments (samples).

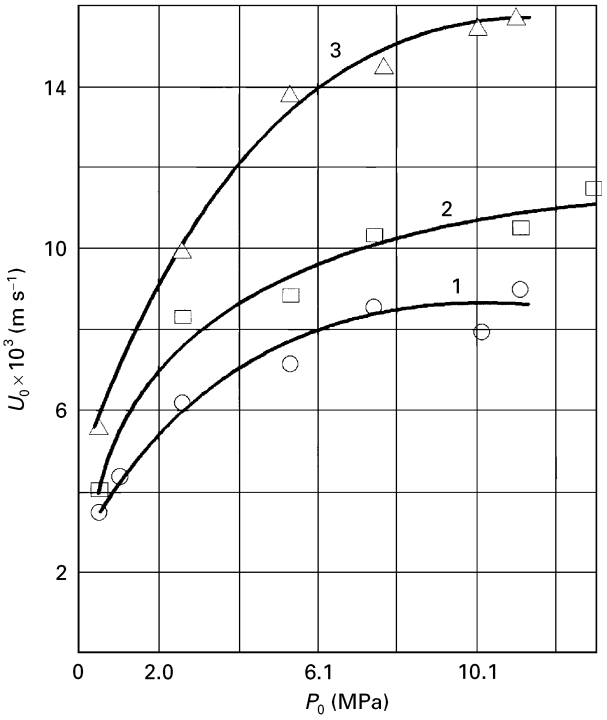

Figure 1 Combustion velocity, U_0, as a function of initial pressure, P_0. $d_{CrO_3} < 300$ μm, $d_{Cr} < 120$ μm. (1) $\alpha = 0.32$, (2) 0.34, (3) 0.5.

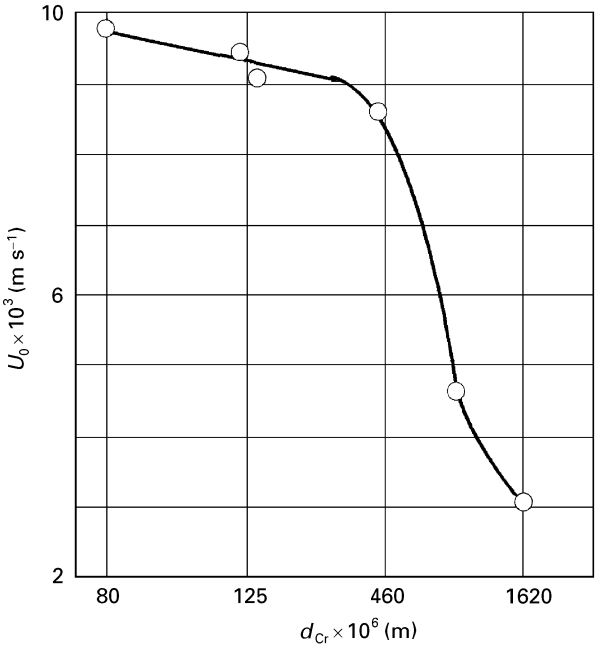

Figure 3 Dependence of combustion velocity, U_0, on chromium particle size, d_{Cr}. $d_{CrO_3} < 300$ μm, $d_{Cr} < 120$ μm, $P_0 = 5.1$ MPa, $\alpha = 0.34$.

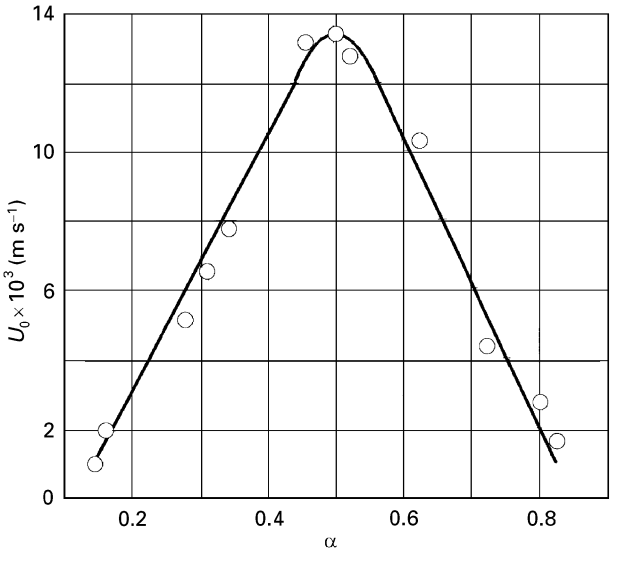

Figure 2 Combustion velocity, U_0, as a function of chromium mass portion, α. $d_{CrO_3} < 300$ μm, $d_{Cr} < 120$ μm, $P_0 = 5.1$ MPa.

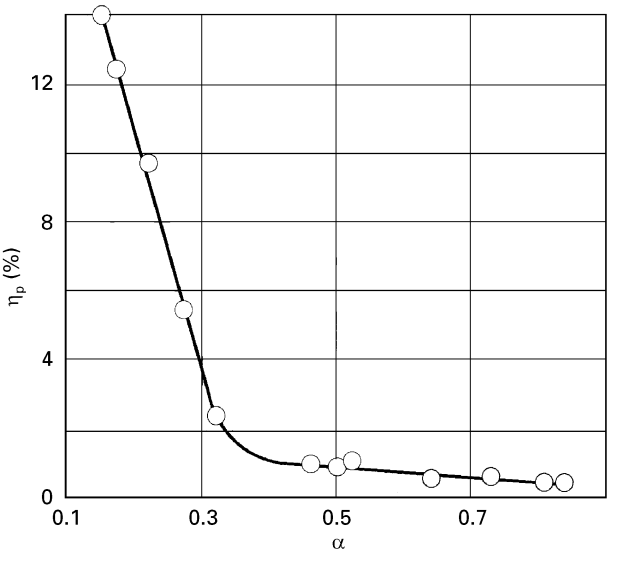

Figure 4 Depth of mixture spraying, η_p, as a function of chromium mass portion, α. $d_{CrO_3} < 300$ μm, $d_{Cr} < 120$ μm., $P_0 = 5.1$ MPa.

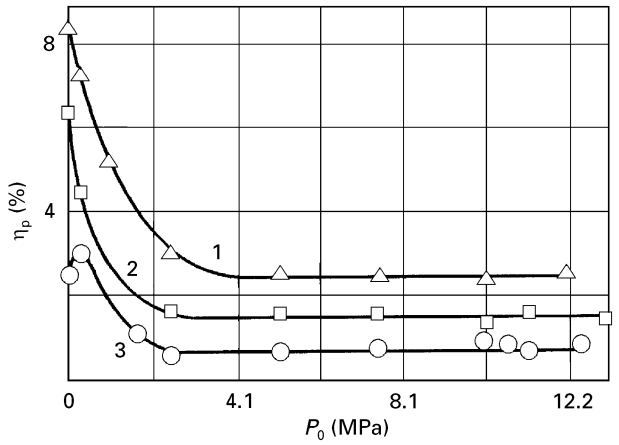

Figure 5 Depth of mixture spraying, η_p, as a function of initial pressure P_0. $d_{CrO_3} < 300$ μm, $d_{Cr} < 120$ μm. 1 — $\alpha = 0.32$; 2 — 0.34; 3 — 0.5.

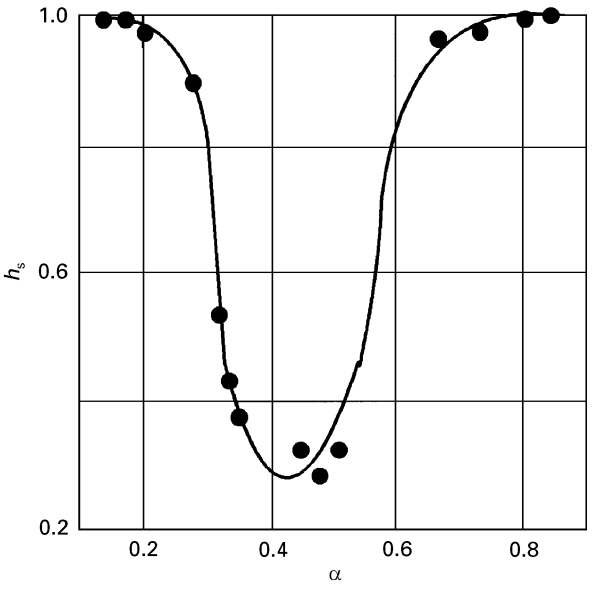

Figure 6 Sample shrinkage, h_s as a function of chromium mass portion, α. $d_{CrO_3} < 300$ μm, $d_{Cr} < 120$ μm, $P_0 = 5.1$ MPa.

3. Results

3.1. Combustion regularities

U_0 changes from 0.6 mm s^{-1} to 16 mm s^{-1} depending on the values of P_0, d_{CrO_3} and α (Figs 1–7).

U_0 increases when P_0 increases for $\alpha = 0.32$, 0.34 and 0.5 (Fig. 1). The relation between U_0 and P_0 can be satisfactorily expressed as

$$U_0 = A(\alpha)P_0^{1/3} \quad (2)$$

where A (the proportional coefficient) is within the range $0.1 < P_0 < 0.5$ MPa camera recording of the combustion velocity is impossible because of smoke.

U_0 as a function of α is shown in Fig. 2. When $\alpha = 0.5$, the velocity, U_0, reaches its maximum and then decreases to combustion termination. A substantial influence of d_{Cr} on U_0 is found within the range $460 < d_{Cr} < 1600$ μm, when the combustion velocity decreases three times reaching the combustion limit (Fig. 3).

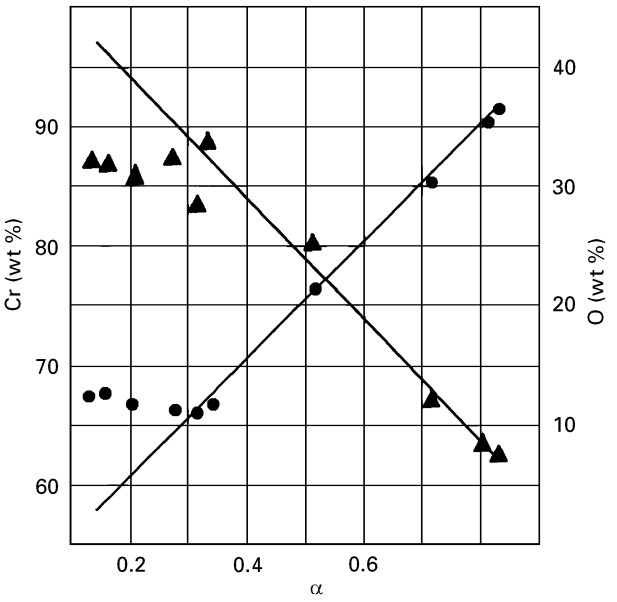

Figure 7 Chemical compositions of the combustion products as functions of chromium mass portion, α. (▲, ●) experimental data, (——) calculated results. $d_{CrO_3} < 300$ μm, $d_{Cr} < 120$ μm, $P_0 = 5.1$ MPa. (▲) chromium, (●) oxygen.

3.1.1. Mixture spraying regularities

The experimental results show that η_p becomes notable for compositions with $\alpha < 0.3$ (Fig. 4) and increases when $P_0 < 2.0$ MPa (Fig. 5).

3.1.2. The state of aggregation of the combustion products

Observation of melting of the combustion products was determined by the appearance of samples and their shrinkage curves (Fig. 6).

The most considerable densification takes place when $0.3 < \alpha < 0.55$ (Fig. 6). The products appear to be present as monoliths with separate large pores. The pressure and particle size variations do not change the sample appearance. Near the combustion limit, the sample density is practically constant, its strength being sufficiently high.

3.1.3. Regularities of the chemical composition formation

Chemical analysis of the combustion products has shown that for $0.15 < \alpha < 0.34$ the chemical composition remains constant (Fig. 7). The Cr : O ratios in the products correspond with Cr_2O_3 phases. This result has been proved by X-ray diffraction analysis of the products. Thus, it can be stated that all surplus oxygen is removed from the combustion products after oxidation of Cr.

For $0.34 < \alpha < 0.8$, the chemical composition changes (Fig. 7) due to the accumulation of surplus Cr in the combustion products. It should be noted that the experimental and calculated chemical compositions coincide in this area. The calculated composition (Fig. 7) is derived from Equation 1.

TABLE I Data for calculating the Clapeyron–Mendeleev equation

Substance	T^m (K) Melting temperature	T^b (K) Boiling temperature	L^m (kJ mol^{-1}) Specific heat of melting	L^b (kJ mol^{-1}) Specific heat of evoporation	Int[a] (kJ mol^{-1})	C^b_{pf} (J K^{-1} mol^{-1})
Cr	2180 [13]	2495 [14]	21.3 [13]	306.5 [14]	71.3 [13]	50.0 [13]
Cr_2O_3	2705 [13]	3300 [12]	125.0 [13]	484.3	325.4 [13]	170.0 [13]

[a] Int is the integral of heat capacity, c_p, from 298 K up to T^m.
[b] c_{pf} is the heat capacity of liquid Cr_2O_3. Also, the calculated $Q_1 = 552.7$ kJ mol^{-1} is the thermal effect of the chemical reaction, Equation 1; $Q_2 = 1105$ kJ mol^{-1} is the thermal effect of the chemical reaction, Equation (3b), in the gas phase: the heat capacity was evaluated using the well known formulae of thermodynamics [12–14].

The difference between the experimental and calculated chemical compositions for $0.15 < \alpha < 0.32$ is caused by oxygen leakage in the experiment (the system under calculation is supposed to be closed).

3.2. CrO_3–Cr combustion mechanism

It is necessary to define a combustion mechanism of the CrO_3–Cr system to consider the experimental data obtained. At first, let us consider the combustion of a stoichiometric mixture in which $\alpha = 0.34$.

Initially, both reactants of the mixture are solid. The final product of the combustion is liquid Cr_2O_3. Reported data [2] on decomposition of CrO_3, a consequence of transformation of the initial mixture in the combustion wave, can be presented as two stages:

$$2CrO_3 \rightarrow \langle Cr_2O_3 \rangle + 1.5O_2 \quad (3a)$$

$$2Cr + 1.5O_2 \rightarrow \ll Cr_3O_3 \gg \quad (3b)$$

where $\langle Cr_2O_3 \rangle$ and $\ll Cr_2O_3 \gg$ are chromium oxide formed under CrO_3 decomposition and Cr combustion, respectively.

CrO_3 decomposition (Equation 3a) starts when its melting point, $T^m_{CrO_3} = 460$ K [12], is reached. Oxygen forms and propagates among the solid $\langle Cr_2O_3 \rangle$ particles to the chemical transformation zone and makes the combustion of Cr with O_2 possible (Equation 3b). The final equilibrium temperature after the completion of combustion is $T_{eq} = 3300$ K. Calculations of T_{eq} and the maximum temperature of combustion in the gas phase, T_m, were made using the overall chemical reaction equation and elementary thermal balances. The boiling temperatures were calculated using the Clapeyron–Mendeleev equation. The initial data for the calculation are given in Table I.

From correlation of T_{eq} with the melting point of Cr_2O_3 $T^m_{Cr_2O_3} = 2700$ K, we can conclude that, under conditions of thermal homogeneity along the cross-section of the sample, solid $\langle Cr_2O_3 \rangle$ loses its filtration ability long before the chemical reaction is complete. In this situation O_2 arrives at the chemical reaction zone as bubbles having no contacts with metal Cr (Fig. 8). Depending on its state of aggregation, metal Cr can be present in the Cr_2O_3 melt in the form of drops or even gas bubbles (the combustion temperature is much higher than the boiling point for Cr). But in the case of contact loss of the reactant, completeness of the chemical reaction becomes impossible.

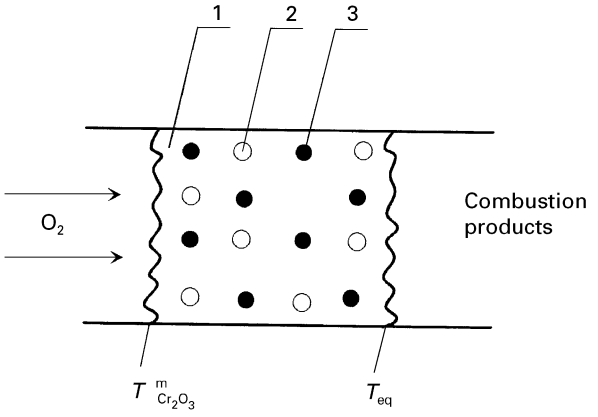

Figure 8 Reactant positions in the chemical reaction zone. (1) liquid Cr_2O_3, (2) O_2, (3) Cr.

The apparent contradiction can be eliminated if we suppose that there is no thermal homogeneity along the cross-section of the sample in the chemical reaction zone and the temperature, $T_{\langle Cr_2O_3 \rangle}$, of the $\langle Cr_2O_3 \rangle$ particles at the moment of completion of the chemical reaction does not exceed $T^m_{Cr_2O_3}$. Thermal inhomogeneity is caused by thermal inertia of the $\langle Cr_2O_3 \rangle$ particles. For the case under consideration, the possible range of $T_{\langle Cr_2O_3 \rangle}$ variation is

$$T^m_{CrO_3} < T_{\langle Cr_2O_3 \rangle} < T^m_{Cr_2O_3} \quad (4)$$

Decreasing $T_{\langle Cr_2O_3 \rangle}$ results in an increase of the combustion product $\ll Cr_2O_3 \gg$, i.e. in overheating. The difference between the temperatures $T_{\langle Cr_2O_3 \rangle}$ and T_m of $\ll Cr_2O_3 \gg$ when the chemical reaction is completing results in a thermal homogenization stage

$$\langle Cr_2O_3 \rangle (T_{\langle Cr_2O_3 \rangle}) + \ll Cr_2O_3 \gg (T_m) \rightarrow Cr_2O_3(T_{eq}) \quad (5)$$

During this homogenization $\langle Cr_2O_3 \rangle$ melts.

For two limiting cases ($T_{\langle Cr_2O_3 \rangle} = T^m_{CrO_3}$ and $T_{\langle Cr_2O_3 \rangle} = T^m_{Cr_2O_3}$) the results of T_m (the maximum combustion temperature in the gas phase) calculations are shown in Fig. 9. From comparison of T_m with the boiling temperatures of $T^b_{Cr_2O_3}$ and T^b_{Cr} it appears that chromium is gaseous in the chemical reaction zone and $T_m \cong T^b_{Cr_2O_3}$. T_m increases with the growth of P_0, γ, the mass portion of gaseous $\ll Cr_2O_3 \gg$ decreases.

On the basis of the above considerations and with the assumption that the chemical reaction zone is narrow in comparison with the heating zone, the

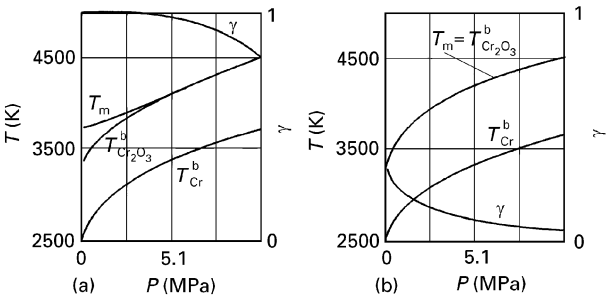

Figure 9 Dependencies of temperatures, T_m, $T^m_{Cr_2O_3}$, T^m_{Cr}, and mass portion of gaseous Cr_2O_3, γ, on pressure, P. (a) $T^m_{Cr_2O_3} = T_{in} = 300$ K, and (b) $T^m_{Cr_2O_3} = T^m_{Cr_2O_3} = 2700$ K.

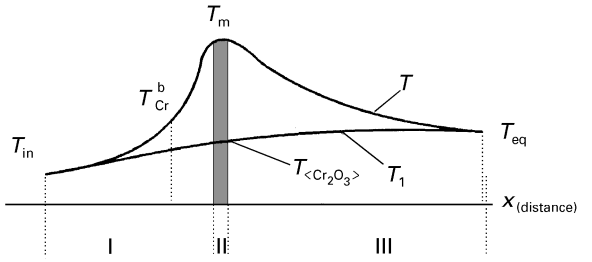

Figure 10 The combustion wave structure for the the gas-phase combustion, where x is the distance.

combustion wave can be presented as in Fig. 10. [T_1 is the temperature of the $\langle Cr_2O_3 \rangle$ particle; the temperatures of the reactants (O_2, Cr) and of the product $\ll Cr_2O_3 \gg$ are equal to T; T_{in} is the initial temperature of the mixture; $\langle Cr_2O_3 \rangle$ and $\ll Cr_2O_3 \gg$ are chromium oxides formed under CrO_3 decomposition and Cr combustion, respectively, see Equation 3a, b.

Three zones can be distinguished in the combustion wave. In zone I the initial mixture heats, CrO_3 decomposes, O_2 filtrates, Cr melts and spreads over. At the boundary of zones I and II Cr is ignited. Subsequent combustion takes place in zone II. Thermal homogenization proceeds in zone III, followed by $\ll Cr_2O_3 \gg$ vapour condensation and $\langle Cr_2O_3 \rangle$ melting.

If we assume that chemical reaction between the Cr drops and O_2 proceeds in a kinetic mode ($\beta \gg k$), and

$$W = k_0 a_2^{n_2} a_3^{n_3} P_0^{\nu} \exp(-E/2RT_m)$$

(where W is the chemical reaction rate; a_2, a_3 are the relative concentrations of O_2 and Cr, respectively; n_2, n_3, ν are the power indeces; k_0 and E are the pre-exponent and the activation energy of chemical reaction (Equation 3b); β and k are the constants of mass transfer and chemical reaction, and R is the universal gaseous constant) then the Cr vaporizes and reacts with O_2 close to the Cr drop surface. Therefore, for such a combustion wave structure the relation between U_0 and P_0 and T_m [15, 16] can be expressed as

$$U_0 = (r_1)^{-1/2} P_0^{(\nu/2)-1} \exp(-E/RT_m) \qquad (6)$$

where r_1 is the radius of the Cr drop after capillary spreading.

Equation 6 is accurate within $T^b_{Cr} \leqslant T_m \leqslant T^b_{Cr_2O_3}$. There can be three cases:

1. $T_m \equiv T^b_{Cr_2O_3}$. Minima diameters of the $\langle Cr_2O_3 \rangle$ particles can be derived from a thermal criterion equation [17, 18] $d_{min} = a\rho/(U_0\rho_1)[12(T^b_{Cr_2O_3} - T^m_{Cr_2O_3})/(T^m_{Cr_2O_3} - T^m_{CrO_3})]^{1/2}$: where the thermal criterion $K = t_1/t_2$; where $t_1 = d_1^2\rho_1/12a\rho$ is the specific time of heating of a spherical particle; $t_2 = x_T/U_0 = a\rho/U_0^2\rho_1$ is the particle residence time in the combustion wave; d_1 and ρ_1 are the particle's diameter and density; x_T is the heating zone length; a and ρ are the gas thermal diffusivity and density.

Using the relation between $T^b_{Cr_2O_3}$ and P_0

$$T^b_{Cr_2O_3} = T_{01} \Big/ \left[\frac{1 - RT_{01}}{L^b_{Cr_2O_3}} \ln(P_0/P_{01})\right] \qquad (7)$$

and assuming that, usually for gas-phase reactions $\nu = 2$, then Equation 6 can be deduced

$$U_0 \sim (P_0/P_{01})^{E/2L^b_{Cr_2O_3}} \qquad (8)$$

Here Equation 7 is a Clausius–Clapeyron equation: T_{01} is the boiling temperature at $P = P_{01}$.

2. $T_m \equiv T^b_{Cr}$. Then

$$U_0 \sim (P_0/P_{01})^{E/2L^b_{Cr_2O_3}} \qquad (9)$$

3. $T^b_{Cr} < T_m < T^b_{Cr_2O_3}$. In this case

$$T_m = T_{00} + Q/c\left[1 + \frac{\alpha_0}{(1-\alpha_0)}(K+1)\right]^{-1} \qquad (10)$$

where $T_{00} = T_{in} - \sum \alpha_i L_i/c_i$ is the reduced initial combustion temperature and α_0 is the mass portion of $\langle Cr_2O_3 \rangle$ in the combustion products.

When $T_m < T^b_{Cr}$ chemical reaction proceeds between O_2 and liquid Cr and combustion occurs by a filtration mechanism [19, 20].

4. Discussion

As shown above, the combustion of a stoichiometric CrO_3–Cr mixture can proceed in a gas-phase mode. The boundary of the gas-phase mode is defined from minimal values of $\langle Cr_2O_3 \rangle$ particles, d_{min}. Substituting the values of the parameters in the equation for d_{min} inside the pressure range 0.1–10 MPa we can evaluate the values of the limit of combustion: $d_{min} = 1.7$–3.4 μm.

Initial CrO_3 particles, with particle size, $d < 300$ μm, were used in the experiments with stoichiometric mixtures. It can be assumed that during decomposition of CrO_3, $\langle Cr_2O_3 \rangle$ particles of similar size form. Therefore, the gas-phase model can be used to consider the experimental results. After comparing U_0 and P_0 relations experimentally (Equation 2) and theoretically (Equation 8), we can conclude that they are similar. The value of the activation energy of the CrO_3–Cr combustion system can be evaluated from the correlation between Equations 2 and 8: $E/2L^b_{Cr_2O_3} \approx 1/3$

$$E = 2/3 L^b_{Cr_2O_3} = 484.3 \times 2/3 \approx 320 \text{ kJ mol}^{-1} \qquad (11)$$

It should be noted that the value of E is close to the specific heat of Cr vaporization ($L^b_{Cr} = 306.5$ kJ mol^{-1}).

The large value of E substantiates the assumption about a narrow zone of chemical reaction between Cr and O_2. The data for the chemical analysis of the products confirm the existence of the narrow chemical reaction zone (Fig. 7) where consumption of oxygen is 100% for the stoichiometric and surplus Cr compositions.

Within a wide range of Cr particle sizes, U_0 is practically constant (Fig. 3). This appears to be due to the fact that capillary spreading of the chromium liquid drops, which were various in their size, resulted in the formation of drops with approximately similar radii. For $d_{Cr} < 460$ μm, U_0 decreases. This occurs due to increases in the capillary spreading time in comparison with the time of residence in the heating zone, and the process does not proceed in a kinetic mode.

The influence of P_0 on U_0 for non-stoichiometric compositions is analogous to that for stoichiometric ones (curves 1 and 3, Fig. 1). For the composition with $\alpha = 0.32$, this similarity is connected with a small difference in the composition. Thus, the relation between U_0 and P_0 is the same as in Equation 8. For a larger deviation from the stoichiometric composition ($\alpha = 0.5$), the calculation produces $T_m = T^b_{Cr}$. For this case the relation between U_0 and P_0 is as given in Equation 9.

An increase in the combustion velocity with increasing α is determined by growth of the combustion temperature, T_m. Further growth of U_0 beyond the stoichiometric value and its passage through a maximum is defined by competition between two factors, i.e. the thermal diffusivity, a, increase and the decrease in T_m. This fact has been noted for other analogous systems [21].

4.1. Formation of structure

It has been shown above that there are two combustion modes:

1. a "hot" mode, when the heat of the chemical reaction is great enough to melt all the reaction products ("cold" and "hot" Cr_2O_3); and
2. a "cold" mode, when "cold" Cr_2O_3 (formed as a result of the decomposition of CrO_3) stays solid during the whole period of the process.

In the first case the final products form from the homogeneous melt. Under this condition, sharply cut and tightly packed grains are formed. Besides, in the cast sample there are separate large pores (Fig. 11a). In the second case the situation is much more complicated. The initial CrO_3 particles disintegrate into smaller pieces of Cr_2O_3, and then products of the reaction between Cr and O_2 condense onto these intermediate particles. The particles formed under combustion of Cr and O_2 and condensed into the porous space are for fewer than the particles formed under CrO_3 disintegration (Fig. 11b).

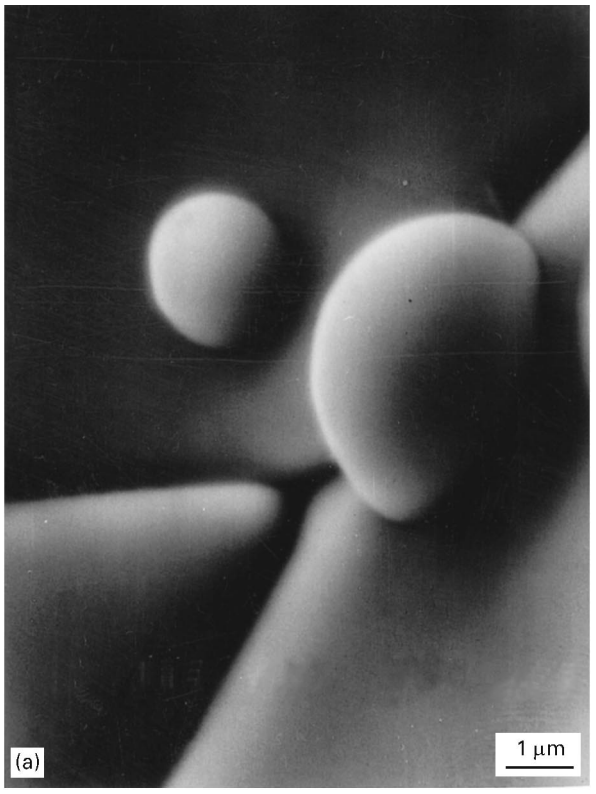

Figure 11 Microphotographs of the combustion products. (a) complete melting, (b) incomplete melting.

4.1.1. Mathematical formulation

Let us consider the process only when all the products have been melted. Then it proceeds as follows. The first stage involves heating up, intensive chemical reaction and an increase in temperature up to and above the melting point of the final Cr_2O_3 product. In the second stage, the Cr_2O_3 formed and the "cold" Cr_2O_3 melt. During the third stage, crystallization of solid Cr_2O_3 from the homogeneous melt occurs.

Due to a sufficiently long period of existence of the homogeneous liquid melt, the system "forgets" its

prehistory, i.e. there are no nuclei or other centres of crystallization that are determined by previous solid structures. Thus, the chemical stage can influence the crystallization (and, consequently, the final structure) only through a temperature field. Therefore, it is sufficient to describe the chemical reaction as an overall one using the constants obtained above in the combustion experiment: i.e. as an activated homogeneous process of first order ("initial reactants" → "final products").

The system in which all the initial and final substances are liquid at the combustion temperature, T_c, is considered. The reaction products are assumed to form in the liquid phase, probably in the overcooled state. Only the reaction products may crystallize in and after the combustion wave. The crystallization heat of the final product is taken into consideration in the heat balance equation. Thus, the process can be presented schematically:

$$\text{initial green mixture} \rightarrow \text{(chemical reaction)} \rightarrow \text{final liquid}$$
$$\text{products} \rightarrow \text{(crystallization)} \rightarrow \text{solid sample (microstructure)}$$

There is always a gap between the general mass of the product and its mass in the solid state.

Formation of the microstructure of the final product is considered using the macrokinetic approach [22–25]. It is assumed that in the homogeneous melt of the final product the nuclei are created spontaneously and then they grow in the kinetic mode (without diffusion limitations). The driving force of the crystallization is undercooling ΔT (the difference between the melting point, T^m, and the current temperature, T), $\Delta T = T^m - T$.

The rates of nucleation, $F_n = \partial N/\partial t$, and grain growth, $F_v = \partial r/\partial t$ (where N is the number of particles of the product, r is the current radius of each particle) are supposed to be linear in respect to the undercooling [26, 27]

$$\begin{aligned} F_n &= K_n(\Delta T - \Delta T_{ms}) \qquad \Delta T > \Delta T_{ms} \\ F_n &= 0 \qquad \Delta T < \Delta T_{ms} \\ F_v &= K_v \Delta T \\ F_n &= F_v = 0 \qquad T > T^m \end{aligned} \tag{12}$$

where ΔT_{ms} is the metastability range (nucleation threshold), i.e. the critical undercooling beyond which nucleation stops; K_n and K_v are the (empirical) crystallization constants.

The final product concentration as well as all the concentrations of all other components are calculated for every moment of time. The nucleation is not instant and the growth rate changes in time with the undercooling. Thus the grain size distribution, N versus r, is not uniform. The calculation of such distributions (microstructure of the material) in different points of the sample is the main and final aim of our numerical analysis.

A well known one-dimensional model of combustion without gas, with a first-order chemical reaction [28] followed by crystallization of the reaction products, is discussed. The thermophysical parameters (heat capacity, c; density, ρ; coefficient of conductivity, λ) are supposed to be constant and equal for both liquid and solid phases (the assumption commonly made in the physics of metals [27]). One side of the sample (layer) is thermally isolated, the other side has a constant temperature, T_w, equal to or more than the temperature of the surrounding medium, T_0 (see Fig. 12). Profiles of the temperature, T_0, versus distance, x, concentration, η_0, versus distance, x, and volume of the crystal phase, V_0, versus distance, x, corresponding to the stationary combustion wave are chosen as the initial conditions. They are calculated before the main numerical solution starts.

Taking into consideration all the above-mentioned and the initial and boundary conditions, the following set of equations can be written for

1. Heat balance.

$$c\rho \frac{\partial T}{\partial t} = \lambda \frac{\partial^2 T}{\partial x^2} + Q(1-\eta)k_0 \exp\frac{-E}{RT} + L^m \rho \frac{\partial V}{\partial t} \qquad 0 < x < h \tag{13}$$

where the left part is the temperature change in time; the first right term is the heat conduction transfer, the second term is the heat of the chemical reaction, the third term is the heat of the phase transition (precipitation).

2. Mass balance on reactant consumption

$$\frac{\partial \eta}{\partial t} = (1-\eta)k_0 \exp\left(\frac{-E}{RT}\right) \tag{14}$$

and mass balance on solid phase (crystal growth) as the Kolmogrov–Avrami formula [22, 27, 29–31] taking into consideration the change in the crystallizing phase volume and valid up to 90–95 vol % concentration

$$V = \left\{1 - \exp\left[-\varphi \int_0^t F_n \left(\int_{t^*}^t F_v \, dt_1\right)^3 dt^*\right]\right\}\eta \tag{15}$$

for $x = 0$:

$$T = T_w \qquad \text{for } x = h\text{: } \frac{\partial T}{\partial x} = 0 \tag{16}$$

for $t = 0$:

$$T = T_0(x) \qquad \eta = \eta_0(x)\text{: } V = V_0(x) \tag{17}$$

Here η is the chemical conversion; t is the time; x is the co-ordinate; Q is the heat effect of chemical reaction;

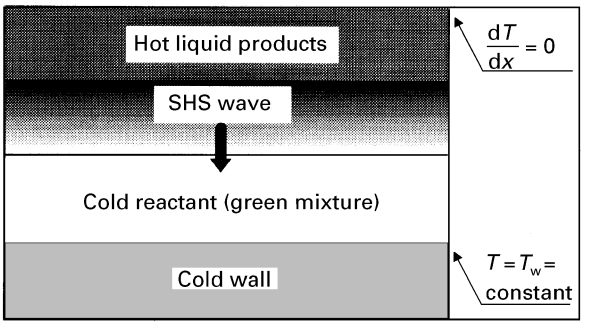

Figure 12 Model scheme of SHS process.

k_0 is the pre-exponent; E is the activation energy of chemical reaction; L^m is the heat of crystallization; T_W is the cold wall temperature; h is the sample length; φ is the form factor, $\varphi = 4/3\ \pi$ for spheres.

4.1.2. Numerical analysis

The set of Equations 12–17 is solved numerically.

The parameters of the problem are chosen for the system under consideration. The values of the kinetic constants of crystallization are absent in the literature. We have made the evaluation from image analysis of metallographic specimens: $K_v = 10^{-5}\,m\,s^{-1}\,K$ and $K_n = 5 \times 10^{10}\,l\,m^{-3}\,s\,K$ with a precision of about a decimal order. $\Delta T_{ms} = 20$ K. The maximum combustion temperature is limited by the boiling point of Cr_2O_3: $T_c = T_{eq} = T^b_{Cr_2O_3} = 3300$ K. The melting point of the product, $T^m = 2705$ K.

As shown above, combustion proceeds in the stationary wave mode (Fig. 13). Together with the combustion wave [the temperature, T, versus distance, x, and the concentration, η, versus distance x, profiles] the undercooling, ΔT versus distance, x, profile moves. During stationary propagation of the combustion wave, the chemical reaction proceeds mainly above the melting point of Cr_2O_3 [15]. Thus, the product Cr_2O_3 forms as a liquid above T_m and crystallization does not occur. The reaction product crystallizes long after the chemical reaction terminates. In this "stationary" zone (see Figs 13 and 14) crystallization proceeds in the "normal" inert mode [25], as if there is no any chemical reaction.

When the combustion wave collides with the cold surface (a copper plate under the sample), extinction takes place: the combustion stops, the temperature along the sample decreases, the temperature profile is restructured. Due to intensive heat removal into the cold wall an under-reacted zone with $\eta < 1$ appears. Thus, near the cold wall, some transient processes and structures are observed.

The new undercooling profile forms and propagates from the cold to the hot end of the sample (Fig. 14). In this case, the Cr_2O_3 product forms beyond the melting

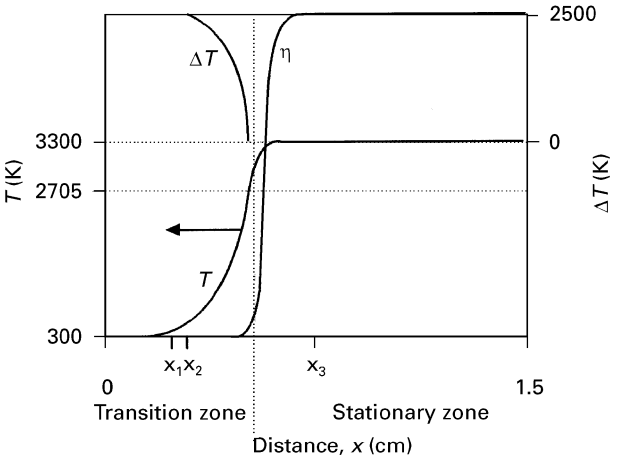

Figure 13 Stationary combustion wave propagation: (T) temperature; (η) product concentration, (ΔT) undercooling. Arrows show the direction of motion of the undercooling waves. Points x_1, x_2 and x_3 on the abscissa axis are the points of the sample.

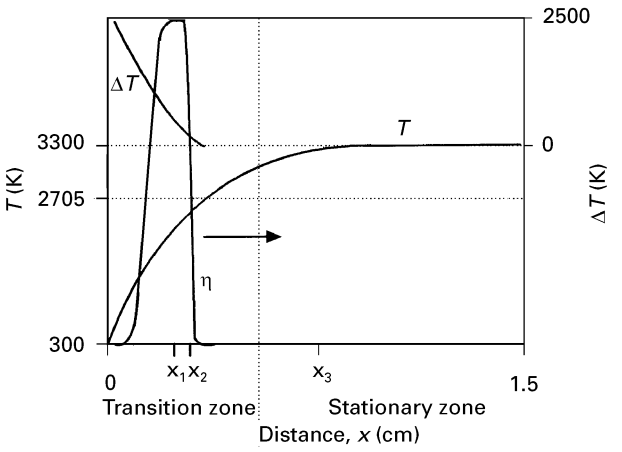

Figure 14 Formation of new undercooling profile and its propagation (inert cooling of the sample). (T) temperature, (η) product concentration, (ΔT) undercooling. Arrow show the direction of motion of the undercooling waves. Points x_1, x_2 and x_3 on the abscissa axis are the points of the sample.

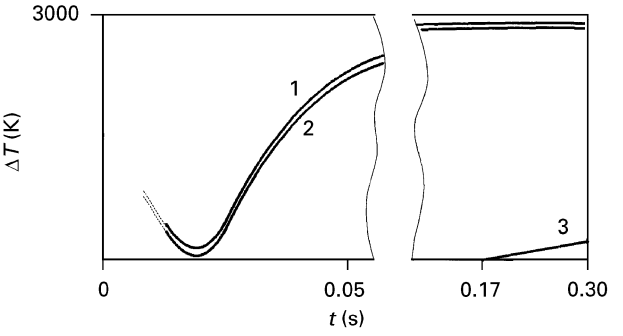

Figure 15 Undercooling, ΔT, development at different points of the sample. (1) $x_1 = 1.5 \times 10^{-3}$ m, (2) $x_2 = 1.8 \times 10^{-3}$ m, (3) $x_3 = 7.5 \times 10^{-3}$ m.

point, T^m, and partly crystallizes in the combustion wave (points 1 and 2 on Fig. 14). In this transition zone the undercooling "wave" propagates in two directions: first to the wall [a primary ΔT versus distance, x, wave coupled with the combustion wave] and then from the wall (a secondary ΔT wave, i.e. "normal" one-dimensional crystallization). The development of undercooling in different parts is shown in Fig. 15: the left branch of the ΔT versus x curve is due to the primary undercooling wave and the right branch is the result of the secondary undercooling wave propagation.

Under reverse motion of ΔT versus x (a secondary undercooling wave) the chemical reaction heats up the Cr_2O_3 crystals formed in the transition zone (Fig. 14) but does not melt them ($T < T^m$). For our parameter in the calculations and for our experiment the width of this transition zone is about $2–3 \times 10^{-3}$ m. Further, the reaction terminates, the sample cools, and crystallization of the non-consumed Cr_2O_3 part starts. As a result, an extraordinary shape of the particle size distribution in the transition zone is observed (Fig. 16). Due to the existence of two stages of crystallization the microstructure, N versus r of the transition zone can be bimodal (Fig. 16, curves 1–3). The right (major "r") mode corresponds to the first stage of crystallization, i.e. to the motion of the

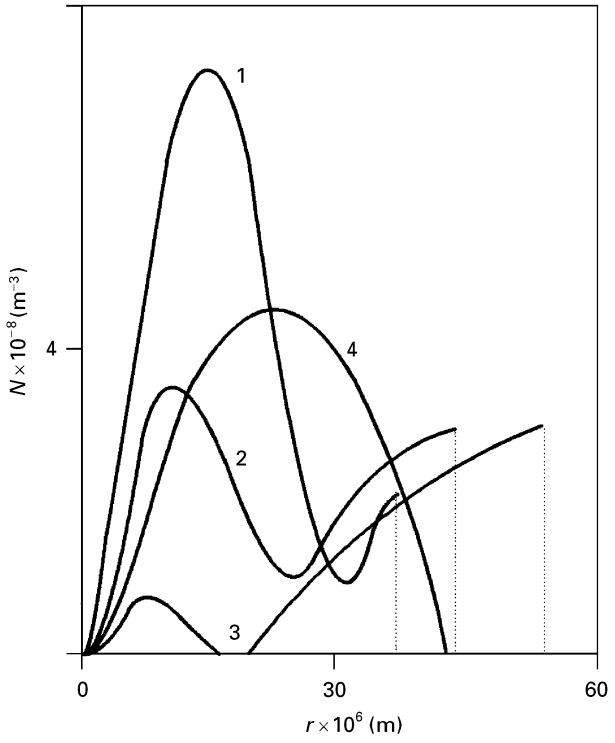

Figure 16 Particle size distributions at various crystallization constants, K_v, K_n. Invariant $K_n K_v^3$ values: (1) $2 \times 10^{-5}\,s^{-4}\,K^4$, (2) $2 \times 10^{-4}\,s^{-4}\,K^{-4}$, (3) $2 \times 10^{-3}\,s^{-4}\,K^4$, (4) $2 \times 10^{-2}\,s^{-4}\,K^4$.

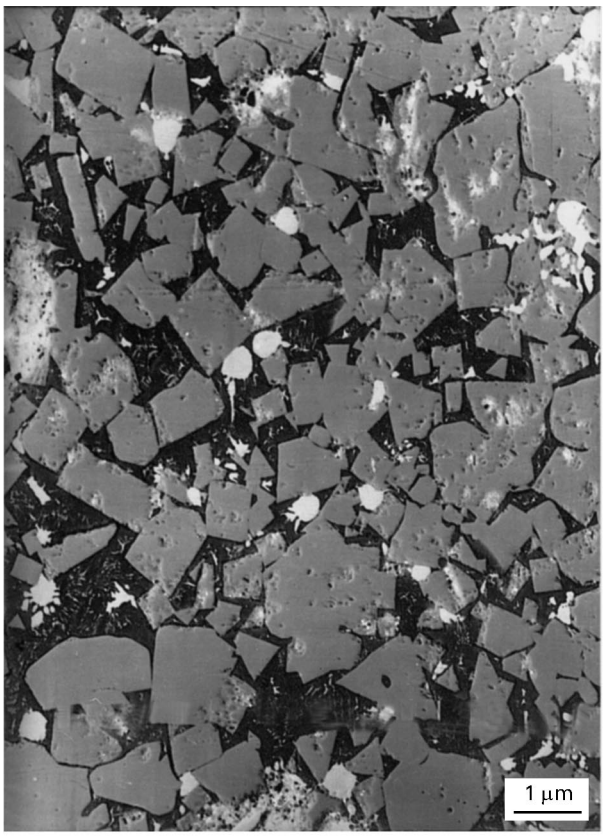

Figure 17 Typical metallographic specimen of $Cr–CrO_3$ system.

undercooling profile to the cold-wall primary-undercooling wave), (Fig. 13). The left mode of N versus r (minor "r") is formed during the second stage of crystallization, i.e. by motion of the undercooling profile from the cold-wall secondary-undercooling wave, (Fig. 14).

After the transition zone (to the right of Fig. 14), crystallization proceeds in the inert mode and "normal" unimodal N versus r distribution forms (curve 4, Fig. 16).

The shape of the N versus r curve in the transition zone is considerably dependent on the crystallization constants K_v and K_n. A special analysis has revealed this dependence on the invariant constants $K_n K_v^3$ (Fig. 16).

Let us consider the process at a fixed point in the transition zone. Under a small values of the invariant constants K_n and K_v^3, the intensity of crystallization is low and crystals that form during the first stage of crystallization have no time to consume a considerable part of the overall volume (amount) of Cr_2O_3 created (curve 1, Fig. 16). Under larger values of K_n and K_v^3, crystallization proceeds almost completely during the first stage. Thus, there is a small amount of Cr_2O_3 for the second stage. As a result the right N versus r mode is equal to or more than the left one (curves 2 and 3, Fig. 16). There can be a situation of partial melting after the first stage (curve 3). Further growth of the invariant constants K_n and K_v^3 results in an increase of the intensity of heat released during crystallization, in a shift of the transition zone to the cold wall and in the formation of a unimodal "normal" distribution, N versus r (curve 4).

The range of the bimodal distribution is rather small (in the space of the sample) and it is difficult to observe this type of N versus r in the experiments (Fig. 17). To produce metallographic specimens with distinct grain structure, special mixtures were used: (CrO_3 + Cr-stoichiometric) + SiO_2, with the ratio 95 : 5. We have found a similar distribution (Fig. 18a). Accordingly, in the two stage crystallization mechanism described above, bimodal distribution can be formed in the transition zone. Moving away from the cold wall (copper plate) we observe a unimodal microstructure with the predominance of the small fraction (Fig. 18b). At last, at a large distance from the plate there is unimodal distribution and the maximum shifts to a larger size of "r" (Fig. 18c).

We have made rough evaluations of the crystallization constants from comparison of experimental and calculated distributions of N versus r for metallographic specimens of SHS-produced Cr_2O_3. The results of calculation for different values of co-ordinate "x" with these values of the crystallization constants, K_n and K_v, and experimental particle size distributions for the same co-ordinates are shown in Fig. 18.

It is seen that the shapes of the distributions are similar experimentally and theoretically. The deformation tendencies of N versus r are the same along the co-ordinate (removal from the cold surface). Therefore, the conclusion can be made that the model considered does reflect the main features of the structural formation process.

5. Conclusions

1. The model $Cr–CrO_3$ SHS system has been studied experimentally and theoretically. The main

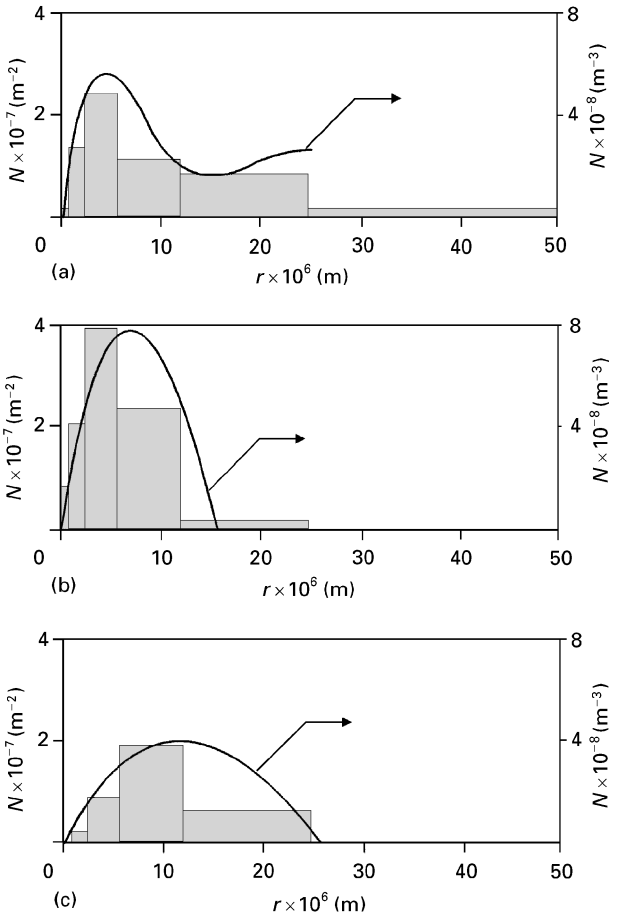

Figure 18 Particle size distributions, $N(r)$, at different points of the Cr_2O_3 sample. (a) $x_1 = 1.5\times10^{-3}$ m, (b) $x_2 = 1.8\times10^{-3}$ m, (c) $x_3 = 7.5\times10^{-3}$ m. Histogram, experiment; curve, calculation.

features of combustion and structure formation have been revealed. Coincidence between experimental data, theoretical analysis and calculated results has been obtained.

2. An unusual combustion model has been developed and approved (for known combustion thermite systems, "metal–metal oxide"). The main stage of the process that determines the combustion velocity is a gas-phase reaction. It is followed by product condensation and melting.

3. For the case of complete melting a mathematical model of the structure formation has been developed and approved. There are two types of product structures: (i) a stationary structure similar to the inert "normal" structure, and (ii) a non-stationary structure in the transition zone near the cold wall. The "normal" particle size distribution in this zone can be strongly deformed up to a bimodal particle size distribution.

Acknowledgements

This work was supported by the Russian Foundation of Fundamental Researches, grant Nos 93-03-18021 and 93-03-09676.

References

1. A. G. MERZHANOV, in "Combustion and plasma synthesis of high-temperature materials", edited by Z. A. Munir and J. B. Holt (VCH, NY, 1990) pp. 1–53.
2. *Idem., Int. J. Self-Propag. High-Temp. Synthesis* **2**(2) (1993) 113.
3. Z. A. MUNIR and U. ANSELMI-TAMBURINI, *Mater. Sci. Reports* **3**(7,8) (1989) 277.
4. J. SUBRAHMANYAM and M. VIJAYAKUMAR, *J. Mater. Sci.* **27** (1991) 6249.
5. V. I. YUKHVID, *Pure Appl. Chem.* **64**(7) (1992) 977.
6. I. P. BOROVINSKAYA, *ibid.* **64**(7) (1992) 919.
7. R. KIEFFER and F. BENESOVSKY, "Hartstoffe" (Springer Verlag, Viena, 1963) 1–384.
8. N. P. LYAPISHEV, Y. L. PLINER, G. F. IGNATENKO and S. I. LAPPO, "Aluminothermics" (Metallurgia, Moscow, 1978) (in Russian) 234–414.
9. A. A. SHIDLOVSKY, "Fundamentals of pyrotechnics" (Mashinostroenie, Moscow, 1973) (in Russian) 63–109.
10. J. H. McLAIN, "Pyrotechnics" (The Franklin Institute Press, Philadelphia, pA 1980) 1–40.
11. J. A. CONKLING, "Chemistry of pyrotechnics" (Marcel Dekker, Inc., N.Y. 1985) 1–35.
12. G. V. SAMSONOV, A. L. BORISOVA, T. G. ZHIDKOVA, T. N. ZNATOKOVA, Y. P. KALOSHINA, A. F. KISELEVA, P. S. KISLY, M. S. KOVALCHENKO, T. Y. KOSOLAPOVA, Y. F. MALAKHOV, V. Y. MALAKHOVA, A. D. PANASYUK, V. I. SLAVUTA and N. I. TKACHENKO, "Physico-chemical properties of oxides" (Metallurgia, Moscow, 1978) (in Russian) 62.
13. V. P. GLUSHKO, I. V. GURVICH, G. A. BERGMAN, I. V. VEITS, V. A. MEDVEDEV, G. A. KHACHKURUZOV and V. S. YUNGMAN, "Thermodynamical properties of individual substances", Vol. 4 (Nauka, Moscow, 1982) pp. 2, 12, 13, 22 (in Russian).
14. U. D. VERYATIN, B. P. MASHIREV, N. G. RYABTSEV, B. I. TARASOV, B. D. POGOZKIN and I. V. KOROBOV, "Thermodynamical properties of inorganic substances" (Atomizdat, Moscow, 1965) p. 64 (in Russian).
15. Y. B. ZELDOVICH, G. I. BARENBLAT, V. B. LIBROVICH and G. M. MAKHVILADZE, "The mathematical theory of combustion and explosion" (Consultants Bureau, NY, 1985).
16. O. N. LEJPUNSKY, *Zhurnal Fizicheskoy Khimii* **1** (1960) 34 (in Russian) 90–96.
17. E. N. RUMANOV and B. I. KHAIKIN, in Procedings of the Third Combustion and Explosion Symposium, edited by L. N. Stesik (Nauka, Moscow, 1972) pp. 161–5 (in Russian).
18. V. I. YUKHVID, E. I. MAKSIMOV and S. I. MATVEEV, in "Combustion and explosion" (Nauka, Moscow, 1977) pp. 236–43 (in Russian).
19. A. P. ALDUSHIN, A. G. MERZHANOV and B. I. KHAIKIN, *Dokl. AN SSSR* **216**(3) (1974) 612 (in Russian).
20. A. P. ALDUSHIN and B. S. SEPLYARSKY, *Fizika goreniya i vzryva* **3** (1976) 323 (in Russian).
21. E. I. MAKSIMOV, A. G. MERZHANOV and V. N. SHKIRO, *ibid.* **4** (1965) 24 (in Russian).
22. P. V. ZHIRKOV, A. Y. DOVZHENKO and E. L. BURAVOVA, *Int. J. Self-Propag. High-Temp. Synthesis* **1**(2) (1992) 222.
23. A. Y. DOVZHENKO and P. V. ZHIRKOV, *Phys. Met. Metallog.* **73** (1992) 5.
24. P. V. ZHIRKOV, A. Y. DOVZHENKO, *Chem. Eng. Sci.* **49** (1994) 2671–2680.
25. A. Y. DOVZHENKO and P. V. ZHIRKOV, *Phys. Met. Metallog.* **76**(3) (1993) 119.
26. A. A. CHERNOV and H. MULLER-KRUMBHAAR (editors), "Modern theory of crystal growth, properties and application" (Springer, Berlin, 1983) 317.
27. G. F. BALANDIN, Fundamentals of theory of casting formation (Mashinostroenie, Moscow, Russia, 1979) (in Russian) 229.
28. A. G. MERZHANOV and B. I. KHAIKIN, *Prog. Energy Combust. Sci.* **14** (1988) 1.
29. M. AVRAMI, *J. Chem. Phys.* **7**(12), (1939) 1103.
30. *Idem*, *ibid.* **8**(2) (1940) 212.
31. *Idem*, *ibid.* **9**(2) (1941) 177.

Received 22 May 1995
and accepted 17 July 1996